Dynamic analysis of fretting-wear in friction contact interfaces

L. Salles, L. Blanc, F. Thouverez, A. M. Gouskov

Dynamic analysis of fretting-wear in friction contact interfaces

L. Salles[a,b,c], L. Blanc[a], F. Thouverez[a], A.M. Gouskov[b]

[a] *École Centrale de Lyon, Laboratoire de Tribologie et Dynamique des Systèmes, Équipe Dynamique des Structures et des Systèmes, 36 avenue Guy de Collongue, 69134 Ecully Cedex, France*
[b] *Department of Applied Mechanics, Bauman Moscow State Technical University, Moscow, Russia*
[c] *Snecma – Safran group, 77550 Moissy-Cramayel, France*

Abstract

A numerical treatment of fretting-wear under vibratory loading is proposed. The method is based on the Dynamical Lagrangian Frequency Time method. It models unilateral contact through Coulomb's friction law. The basic idea is to separate time in two scales, slow scale for tribological phenomena and fast scale for dynamics. For a chosen number of periods of vibration, a steady state is assumed and the variables are decomposed in Fourier series. An Alternating Frequency Time procedure is performed to calculate the non-linear forces. Then, a Hybrid Powell's algorithm is used as solver. Numerical investigations on a beam with friction contact interfaces illustrate the performances of this method and show the coupling between dynamical and tribological phenomena.

Key words: harmonic balance method, friction and contact, fretting-wear

1. Introduction

Friction dampers are widely used in industry and civil engineering to control the vibrations of structures. Friction damping is often obtained via the design of the mechanism, this is the case for example in turbomachinery applications when a bladed disk includes dovetail attachments. The positive effect of such dampers is the decrease of vibrations, but friction also introduces micro and/or macro slip that could be accompanied with fretting-wear. Indeed, some industrial damage surveys have shown that the predictions underestimate wear on long-haul aircrafts' dovetail profiles. This problem has not been encountered on short-haul aircrafts equipped with the same type of engines. Considering that wear predictions have been performed in quasi-static take-off and landing situations, for which vibratory effects are neglected, it is supposed here that a coupling between wear and vibrations occurs during the parts of the flights operated at cruise speed, all the more as these parts last much longer than the others on long-haul aircrafts. An academic example is proposed to illustrate the phenomena that actually matter.

Roughly speaking, the state of the art concerning the modelling and calculation methods available to solve such problems is as follows. On the one hand, recent methods enable one to calculate the vibrational response of bladed disks in the presence of friction in blade attachments [1, 2, 3] but wear is not taken into account, on the other hand most fretting-wear studies are performed in quasi-static situations for which inertial - and then vibratory - effects are neglected. Aside from [4, 5], the coupling between fretting-wear and vibrations is very seldom taken into account in the literature due to the complexity it introduces.

Wear itself is a complex phenomenon because wear debris creation can be changed by hardness, plasticity, grain structure, temperature, etc. According to [6] around 180 laws of wear have been proposed. To quantify wear, the Archard's model [7] is the most commonly used. It considers that the wear volume is linked to the product of normal force and sliding displacement. Classically, wear coefficient quantification is performed

Email address: loic.salles@ec-lyon.fr (L. Salles)

through the evaluation of the worn volume as a function of the normal load. The loss of matter can be known through the measurement of the loss of mass, of the loss of dimensions, of the evolution of Vickers microhardness imprints or directly by surface profilometry. The Archard's model will be used here.

In the absence of vibratory effects, wear laws are often used with the Finite Element Method (FEM) to solve deformable contact problems and get the evolution of wear rate and worn geometry as post-processing steps in looping procedures. Commercial softwares can be used to model wear-cycles with an external routine to compute wear and remesh the geometry [8, 9]. This strategy is highly time consuming. In order to reduce the calculation costs some simplified approaches have been developed based on Winkler's foundation to predict wear [10]. Various approaches have also been proposed to predict wear based on semi-analytical models [11] or on Boundary Elements Methods (BEM) [12]. The later has been coupled with an optimization technique [13] to get directly the worn geometry. Semi-analytical methods and BEM are very difficult to use when the problem of contact with friction takes vibratory effects into account.

In this paper, an approach based on the FEM is proposed to model the coupling between fretting-wear and vibration. It is based on the Dynamical Lagrangian Frequency Time method (DLFT) [3] and on a multiscale approach to reduce the computational costs. The main assumption is that a periodic steady state is reached and that wear will modify this state only a little. Thus, it is possible to use methods based on Multi Harmonic Balance and Alternate Frequency Time procedures [14, 15, 2]. A multiscale formalism is introduced to distinguish between the "fast" phenomena caused by vibrations and the "slow" phenomena due to wear. Then, iterative numerical techniques are necessary because a non-linear system must be solved, at each step of the slow scale. Here the strategy is based on a Hybrid Powell's solver. Concerning the treatment of wear through Archard's law, it is assumed that the friction coefficient is unaffected by the evolution of wear. Hardness will be considered constant. The plasticity of the material will be neglected. But more elaborate models, based on the dissipated energy for example [16], could have been used as well.

The first examples treated by this DLFT-with-wear method have appeared in [17] and [18]. Here the formalism is presented more thoroughly and a comparison with an example stemming from the literature is proposed [19].

2. The reference problem

2.1. Continuous formulation

Let us consider an elastic solid Ω in contact with a fixed rigid body Ω_R through a frictional interface Γ_c in situation of fretting-wear (Fig. 1). The boundary of Ω, $\partial\Omega$, is smooth; it is divided into three disjoint parts Γ_t, Γ_u and Γ_c. $\boldsymbol{n}$ designates the unit normal vector outward $\partial\Omega$. Traction forces T excite Γ_t periodically. Displacements U are imposed on Γ_u and frictional contact with fretting-wear conditions on Γ_c. There are no body forces. Ω's material is supposed to be linearly and isotropically elastic. Perturbations are assumed to be small.

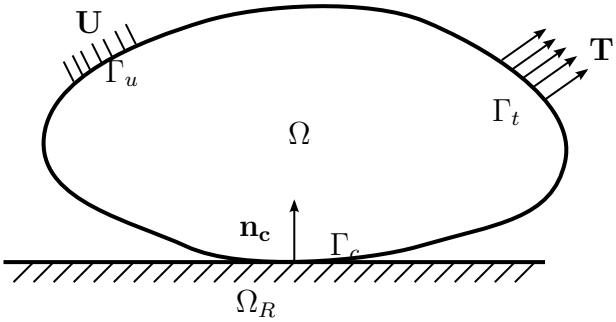

Figure 1. Description of the problem

In the presence of inertial forces, the equations of the problem of elasticity for Ω, excepting the contact interface, are, classically:

$$\mathbf{div}\,\boldsymbol{\sigma} = \rho\,\ddot{\boldsymbol{u}} \qquad \text{in} \quad \Omega, \tag{1}$$

$$\boldsymbol{\sigma}\,\boldsymbol{n} = \boldsymbol{T} \qquad \text{on} \quad \Gamma_t, \tag{2}$$

$$\boldsymbol{u} = \boldsymbol{U} \qquad \text{on} \quad \Gamma_u, \tag{3}$$

$$\boldsymbol{\sigma} = \boldsymbol{E}\boldsymbol{\epsilon} \qquad \text{in} \quad \Omega, \tag{4}$$

where $\boldsymbol{u}$, $\boldsymbol{\sigma}$, $\boldsymbol{E}$ and $\boldsymbol{\epsilon}$ are respectively the field of displacements, Cauchy's stress tensor, Hooke's tensor and the infinitesimal strain's tensor.

The constitutive equations ruling the contact interface are described within the formalism of continuum thermodynamics, following Stromberg's works [19]. Firstly, a specific free energy Ψ is introduced to produce an extension of Signorini's unilateral contact conditions that takes wear into account.

$$\Psi = I_C(u_N, w), \qquad C = \{(u_N, w) : u_N - w - g \leq 0\}\,. \tag{5}$$

I_C is the indicator function of the set C (i.e. $I_C = 0$ if $(u_N, w) \in C$ and $I_C = +\infty$ otherwise). u_N designates the normal component of the interfacial displacement. Wear is introduced as a new state variable w, increasing the initial gap g between the two surfaces in contact. The state laws associated with Ψ make the unilateral contact conditions explicit:

$$\mathcal{W} = p_N \geq 0, \quad u_N - w - g \leq 0, \quad p_N(u_N - w - g) = 0, \tag{6}$$

where $\mathcal{W}$ designates the dual of w i.e. the driving force for wear, which has the same physical meaning as p_N, the normal component of the contact pressure exerted by Ω_R on Ω.

Secondly, the dual $\Phi^\star$ (in the sense of the Legendre-Fenchel transform) of a pseudo-dissipation potential Φ gives Coulomb's law of friction and Archard's law of wear.

$$\Phi^\star = I_{F(p_N)}(\boldsymbol{p_T}, \mathcal{W}), \quad F(p_N) = \left\{(\boldsymbol{p_T}, \mathcal{W}) : \|\boldsymbol{p_T}\| - \mu\,p_N + k_w\,p_N\mathcal{W} - k_w\,p_N^2 \leq 0\right\}. \tag{7}$$

The set $F(p_N)$ is a closed convex set defining the friction and wear limit criteria. $I_{F(p_N)}$ is its indicator function, defined the same way as I_C. $\mathbf{p_T}$ is the tangential component of the contact pressures. $\|.\|$ represents the Euclidian norm. μ and k_w are respectively Coulomb's friction coefficient and Archard's law wear coefficient. This choice of $\Phi^\star$ give the following complementary laws for $\mathcal{W} = p_N \geq 0$:

$$\begin{gathered} \dot{\boldsymbol{u}}_T = \dot{\lambda}\frac{\boldsymbol{p_T}}{\|\boldsymbol{p_T}\|}, \quad \dot{w} = \dot{\lambda}\,k_w\,p_N, \\ \dot{\lambda} \geq 0, \quad \|\boldsymbol{p_T}\| - \mu\,p_N \leq 0, \quad \dot{\lambda}\,(\|\boldsymbol{p_T}\| - \mu\,p_N) = 0 \end{gathered} \tag{8}$$

In (8) can be recognised both a local form of Archard's law of wear and a mathematical definition of the Coulomb's cone in case of fretting-wear.

Variationally, the problem is defined by three integral equations and one constitutive law (9-12). These equations stem from the principle of virtual work, the weak formulation of Signorini's unilateral contact conditions, the complementary law of Coulomb and the local formulation of Archard's law. For each moment t of the studied time interval $[0, T]$, are sought the displacement field $\mathbf{u}$ for each point $\mathbf{x}$ of Ω and the contact pressure field $\mathbf{p}$ (with $p_N = \mathcal{W}$ and $\mathbf{p_T}$ its normal and tangential components). $\mathbf{v}$, $\mathbf{p}'$ and $\mathcal{W}'$ designate the test-fields associated respectively with $\mathbf{u}$, $\mathbf{p}$ and $\mathcal{W}$.

$$\int_{\Omega^l} \rho\ddot{u}_i v_i dV + \int_{\Omega^l} E_{ijkl}\frac{\partial u_k}{\partial x_l}\frac{\partial v_i}{\partial x_j}\,dV \quad + \int_{\Gamma_c} p_i v_i\,dA - \int_{\Gamma_t^l} t_i v_i\,dA = 0 \quad \forall \mathbf{v} \in \mathcal{V}, \tag{9}$$

$$\int_{\Gamma_c} (u_N - w - g)(p'_N - p_N)\,dA \leq 0 \quad \forall p'_N \in \mathcal{K}_N, \tag{10}$$

$$\int_{\Gamma_c} \left(\dot{u}_{T_\alpha}\,(p'_{T_\alpha} - p_{T_\alpha}) + \quad \dot{w}\,(\mathcal{W}' - \mathcal{W})\right)\,dA \leq 0 \quad \forall (p'_T, \mathcal{W}') \in \mathcal{F}(p_N) \tag{11}$$

with

$$\begin{aligned}\mathcal{V} &= \{\mathbf{v} \,|\, \mathbf{v}(\mathbf{x}) = \mathbf{0}, \mathbf{x} \in \Gamma_u\}\,,\\ \mathcal{K}_N &= \{p_N \,|\, p_N(\mathbf{x}) \geq 0, \mathbf{x} \in \Gamma_c\}\,,\\ \mathcal{F}(p_N) &= \{(\mathbf{p_T}, \mathcal{W}) \,|\, (\mathbf{p}_T(\mathbf{x}), \mathcal{W}(\mathbf{x})) \in F(p_N), \mathbf{x} \in \Gamma_c\}\,.\end{aligned}$$

In (11), the components of each vector are expressed in an orthonormal basis $\mathbf{n}_\alpha$, perpendicular to $\mathbf{n}$. $\dot{w}$ is obtained through the following equation:

$$\dot{w} = K_w \left|p_N\right| \left\|\dot{\mathbf{u}}_T\right\| \tag{12}$$

2.2. Finite element discretization

A FEM discretization of (9) is performed. Capital letters designate the FEM counterpart of the variables named by small letters before: they are vectors of nodal quantities. The equations of motion are:

$$\mathbf{M}\ddot{\boldsymbol{U}} + \mathbf{C}\dot{\boldsymbol{U}} + \mathbf{K}\boldsymbol{U} + \boldsymbol{F_c}(\boldsymbol{U}, \dot{\boldsymbol{U}}, \boldsymbol{W}) = \boldsymbol{F_{ex}}, \tag{13}$$

where $\mathbf{M}$, $\mathbf{C}$ and $\mathbf{K}$ respectively designate the mass, damping and stiffness matrices. $\boldsymbol{F_{ex}}$ is the vector of external forces. $\boldsymbol{F_c}$ represents the non-linear contact forces due to friction and impact; they also depend on wear and on materials' properties.

Wear is calculated at each interface node by:

$$\dot{W}^M = \frac{K_w}{\alpha^M} \left|P_N^M\right| \left\|\dot{\boldsymbol{U}}_T^M\right\|. \tag{14}$$

α^M is the weighting factor for node M. The weighting factors depend on the quadrature rule used to calculate the integrals on each elementary contact area. Exponent M in P_N^M and $\dot{\boldsymbol{U}}_T^M$ designate the nodal quantities.

The constraints introduced by equations (10) and (11) become:

$$\begin{aligned}{}^t(\boldsymbol{U}_N - \boldsymbol{W} - \boldsymbol{G})\,(\boldsymbol{P}'_N - \boldsymbol{P}_N) &\leq 0 \quad \forall \boldsymbol{P}'_N \in \mathcal{K}_N^h, &(15)\\ {}^t\dot{\boldsymbol{U}}_T\,(\boldsymbol{P}'_T - \boldsymbol{P}_T) &\leq 0 \quad \forall \boldsymbol{P}'_T \in \mathcal{F}^h(\boldsymbol{P}_N), &(16)\end{aligned}$$

where $\mathcal{K}_N^h = \left\{P_N^M \,|\, P_N^M \geq 0\right\}$ is the approximation of $\mathcal{K}_N$ and $\mathcal{F}^h(\boldsymbol{P}_N) = \left\{\boldsymbol{P}_T^M \,|\, \left\|\boldsymbol{P}_T^M\right\| - \mu|\boldsymbol{P}_N^M| \leq 0\right\}$ is the approximation of $\mathcal{F}(p_N)$ with $\mathcal{W}^M = \boldsymbol{P}_N^M$.

3. The DLFT-with wear method

3.1. A Harmonic Balance Method with two time scales

The strategy belongs to the family of multiscale approaches ([20], [21]). In [22], a time scale separation is also used with an averaging procedure to estimate qualitatively the dynamics of damage evolution. In [23], the wear of a wheel-rail is studied this way.

Here, time is split into two different scales: a fast one associated with vibratory phenomena and a slow one associated with wear. τ and η are respectively the variables of the fast and of the slow time scales. At the scale of a few cycles, wear appears as an almost constant interface gap. It is then assumed that wear doesn't change the aspect of the periodic response during a short lapse of time: on this period it is possible to describe displacements and forces with Fourier series of τ. On a longer duration, Fourier coefficients evolve as functions of η. Anyway, wear doesn't change the pulsation of the response because it is ruled by the pulsation of the excitation, ω, which isn't affected by fretting-wear. η can then be considered as a "large" multiple of the time period $T = \frac{2\pi}{\omega}$ of the fretting-wear cycles.

The Fourier series of $\boldsymbol{U}$ can be expressed as:

$$\boldsymbol{U}(\tau,\eta) = \tilde{\boldsymbol{U}}_0(\eta) + \sum_{n=1}^{N_h} \left(\tilde{\boldsymbol{U}}_{n,c}(\eta)\cos(n\omega\tau) + \tilde{\boldsymbol{U}}_{n,s}(\eta)\sin(n\omega\tau) \right). \tag{17}$$

Afterwards, 17 is summarized by a multi-harmonic frequency-domain vector:

$$\tilde{\boldsymbol{U}}(\eta) = \left[\tilde{\boldsymbol{U}}_0, \tilde{\boldsymbol{U}}_{1,c}, \cdots, \tilde{\boldsymbol{U}}_{N_h,c}, \tilde{\boldsymbol{U}}_{1,s}, \cdots, \tilde{\boldsymbol{U}}_{N_h,s} \right], \tag{18}$$

where c and s respectively stand for "cosine" and "sine".

A Galerkin procedure is then performed to formulate equation 13 in the frequency domain. It is important to mention that, here, the depth of wear is very small compared with the characteristic dimensions of the structures in contact; that is why the modifications of the mass and stiffness matrices due to wear are neglected. 13 becomes:

$$\mathbf{Z}\,\tilde{\boldsymbol{U}}(\eta) + \tilde{\boldsymbol{F}}_c(\eta) = \tilde{\boldsymbol{F}}_{\boldsymbol{ex}}(\eta). \tag{19}$$

$\tilde{\boldsymbol{F}}_c$ and $\tilde{\boldsymbol{F}}_{\boldsymbol{ex}}$ are respectively the multi-harmonic frequency-domain vectors of contact and excitation forces. $\mathbf{Z}$ is a block-diagonal matrix such that:

$$\mathbf{Z} = diag\left(\mathbf{K}, \mathbf{Z}_1, \ldots, \mathbf{Z}_{N_h}\right) \quad \text{with} \quad \mathbf{Z}_n = \begin{bmatrix} \mathbf{K} - (n\omega)^2\mathbf{M} & n\omega\mathbf{C} \\ -n\omega\mathbf{C} & \mathbf{K} - (n\omega)^2\mathbf{M} \end{bmatrix}, \quad n = 1 \ldots N_h \tag{20}$$

In practice, as detailed in [3], the size of the frequency-domain problem is reduced, without loss of information, through a condensation on the interface nodes, which are involved afterwards in the treatment of contact non-linearities [1]. Equation 19 becomes:

$$\mathbf{Z}_{\mathbf{r}}\tilde{\boldsymbol{U}}_{\boldsymbol{r}}(\eta) + \tilde{\boldsymbol{\lambda}}(\eta) = \tilde{\boldsymbol{F}}_{\boldsymbol{r}}, \tag{21}$$

or

$$f(\tilde{\boldsymbol{U}}_{\boldsymbol{r}}) = \mathbf{Z}_{\mathbf{r}}\tilde{\boldsymbol{U}}_{\boldsymbol{r}}(\eta) + \tilde{\boldsymbol{\lambda}}(\eta) - \tilde{\boldsymbol{F}}_{\boldsymbol{r}} = \mathbf{0}, \tag{22}$$

where $\tilde{\boldsymbol{U}}_{\boldsymbol{r}}$, $\tilde{\boldsymbol{F}}_{\boldsymbol{r}}$ and $\mathbf{Z}_{\mathbf{r}}$ designate respectively the reduced multiharmonic relative displacement vector, reduced stiffness matrix and reduced external excitation. $\tilde{\boldsymbol{\lambda}}$ is the vector of the Lagrange multipliers which represent the reduced contact forces in the frequency domain.

Algorithmically, the solution over the time interval $[0, T]$ is calculated through a step-by-step procedure involving an incrementation of the slow time variable: for each step, Eq. 22 is solved through a Newton-like solver; this process constitutes the external loop of the method.

3.2. Modeling of the contact forces

Solving 21 requires to know the expression of $\tilde{\boldsymbol{\lambda}}$. Unfortunately it is not possible to calculate it directly in the Galerkin procedure, indeed it depends on the state of each contact node - stick, slip or separation - which is a priori unknown. To undertake this difficulty it is common to use the Alternating Frequency Time method (AFT) [24]. Displacements and velocities are calculated in the frequency domain and transformed into the time domain using an inverse DFT procedure (iDFT). In the time domain, contact forces could be evaluated through different methods. The easiest one is to regularize the *sign* function - depending on the velocity in the evaluation of Coulomb's forces - by another function which is continuous. It allows a direct computation of the non-linear friction forces [25]. The use of a penalty method is another popular

[1] Another exact reduction would also be used in the case of a contact between two deformable solids, it consists of working on the degrees of freedom associated with the relative displacements at the interface instead of both the displacements of each solid.

method [14, 25, 26, 2, 27, 28]. The additional stiffnesses may then represent a damper's stiffness or the contact asperities stiffness. In the case of fretting-wear theses stiffnesses could change with wear process, to take the modification of material properties in the contact area into account.

Another method has been proposed by Nacivet *et al.* [3]: the Dynamic Lagrangian Frequency-Time method (DLFT). It uses augmented Lagrangians which allow to calculate without any softening of the non-smooth frictional contact law. A time-marching procedure in the time domain is also required. Compared to the conventional contact penalty method, the main advantage of the DLFT method is that, at convergence, results don't depend on any penalty coefficient (hence the term "pseudo-penalty" coefficient to designate the coefficient used below to enforce the matching between the time and frequency descriptions of displacements). For stability reasons, good results are generally obtained when this coefficient is roughly equal to the spectral radius of the dynamic stiffness matrix. This method has been successfully used to predict friction damping in blade attachments [1] and to quantify the efficiency of friction ring dampers [28]. In a precedent paper [17] this method has been coupled with a polynomial expansion of wear to calculate directly the wear evolution for a two-degrees-of-freedom model. Here the formalism for contact forces calculation is the same as in [17] (but wear depth is evaluated in a less complex manner, explained farther).

In the frequency domain, the Lagrange multiplier $\tilde{\boldsymbol{\lambda}}$ is formulated as a pseudo-penalization of the equations of motion on the tangential and normal directions:

$$\tilde{\boldsymbol{\lambda}}^{\boldsymbol{T}} = \tilde{\boldsymbol{F}}_{\boldsymbol{r}}^{T} - \left(\mathbf{Z}_{\mathbf{r}}\tilde{\boldsymbol{U}}_{\boldsymbol{r}}\right)^{T} + \epsilon_T\left(\tilde{\boldsymbol{U}}_{\boldsymbol{r}}^{T} - \tilde{\boldsymbol{X}}_{\boldsymbol{r}}^{T}\right), \tag{23a}$$

$$\tilde{\boldsymbol{\lambda}}^{\boldsymbol{N}} = \tilde{\boldsymbol{F}}_{\boldsymbol{r}}^{N} - \left(\mathbf{Z}_{\mathbf{r}}\tilde{\boldsymbol{U}}_{\boldsymbol{r}}\right)^{N} + \epsilon_N\left(\tilde{\boldsymbol{U}}_{\boldsymbol{r}}^{N} - \boldsymbol{W}^{N} - \tilde{\boldsymbol{X}}_{\boldsymbol{r}}^{N}\right). \tag{23b}$$

ϵ_T and ϵ_N are pseudo-penalty coefficients, $\tilde{\boldsymbol{X}}_{\boldsymbol{r}}$ is a new vector of relative displacements, which is computed in the time domain. The pair $\left(\tilde{\boldsymbol{\lambda}}, \tilde{\boldsymbol{X}}_{\boldsymbol{r}}\right)$ is determinated through an AFT procedure. Equation (22) becomes:

$$f(\tilde{\boldsymbol{U}}_{\boldsymbol{r}}) = \epsilon\left(\tilde{\boldsymbol{U}}_{\boldsymbol{r}} - \boldsymbol{W} - \tilde{\boldsymbol{X}}_{\boldsymbol{r}}\right), \quad \text{with} \quad \epsilon = \epsilon_T = \epsilon_N. \tag{24}$$

The convergence ensures that the time domain $\tilde{\boldsymbol{X}}_{\boldsymbol{r}}$ and frequency domain $\tilde{\boldsymbol{U}}_{\boldsymbol{r}}$ match with respect for contact conditions.

The AFT is based on a prediction/correction procedure in the time domain (summarized in Fig. 2). Algorithmically, this is the internal loop of the method.

The contact forces are calculated in the time domain, where the transition criteria between the three possible states are easily formulated. Equation (23) is reformulated as:

$$\tilde{\boldsymbol{\lambda}} = \underbrace{\tilde{\boldsymbol{F}}_{\boldsymbol{r}} - \mathbf{Z}_r\tilde{\boldsymbol{U}}_{\boldsymbol{r}} + \epsilon\left(\tilde{\boldsymbol{U}}_{\boldsymbol{r}} - \boldsymbol{W}\right)}_{\tilde{\boldsymbol{\lambda}}_{\boldsymbol{u}}} - \underbrace{\epsilon\tilde{\boldsymbol{X}}_{\boldsymbol{r}}}_{\tilde{\boldsymbol{\lambda}}_{\boldsymbol{x}}}, \tag{25}$$

The period is split into N time steps. $\tilde{\boldsymbol{\lambda}}$, $\tilde{\boldsymbol{\lambda}}_{\boldsymbol{u}}$ and $\tilde{\boldsymbol{\lambda}}_{\boldsymbol{x}}$ have $\{\boldsymbol{\lambda}^{\boldsymbol{n}}\}_{n=1..N}$, $\{\boldsymbol{\lambda}_{\boldsymbol{u}}^{\boldsymbol{n}}\}_{n=1..N}$ and $\{\boldsymbol{\lambda}_{\boldsymbol{x}}^{\boldsymbol{n}}\}_{n=1..N}$ as respective time domain counterparts. These vectors are obtained from the frequency domain vectors through an iDFT procedure. A prediction/correction is then used to compute the contact forces. At each time increment it first assumes that the contact node is in stick situation, thus the node doesn't move: $\boldsymbol{\lambda}_{\boldsymbol{x}}^{\boldsymbol{n},\boldsymbol{T}} = \boldsymbol{\lambda}_{\boldsymbol{x}}^{\boldsymbol{n-1},\boldsymbol{T}}$ and $\boldsymbol{\lambda}_{\boldsymbol{x}}^{\boldsymbol{n},\boldsymbol{N}} = 0$. The predicted contact forces are:

$$\boldsymbol{\lambda}_{\boldsymbol{pre}}^{\boldsymbol{n},\boldsymbol{T}} = \boldsymbol{\lambda}_{\boldsymbol{u}}^{\boldsymbol{n},\boldsymbol{T}} - \boldsymbol{\lambda}_{\boldsymbol{x}}^{\boldsymbol{n-1},\boldsymbol{T}}, \quad \lambda_{pre}^{n,N} = \lambda_{u}^{n,N}. \tag{26}$$

The corrected contact forces will be:

$$\boldsymbol{\lambda}^{\boldsymbol{n}} = \boldsymbol{\lambda}_{\boldsymbol{u}}^{\boldsymbol{n}} - \boldsymbol{\lambda}_{\boldsymbol{x}}^{\boldsymbol{n}}, \tag{27}$$

and $\boldsymbol{\lambda}_{\boldsymbol{x}}^{\boldsymbol{n}}$ will we be calculated to satisfy the contact and friction laws.

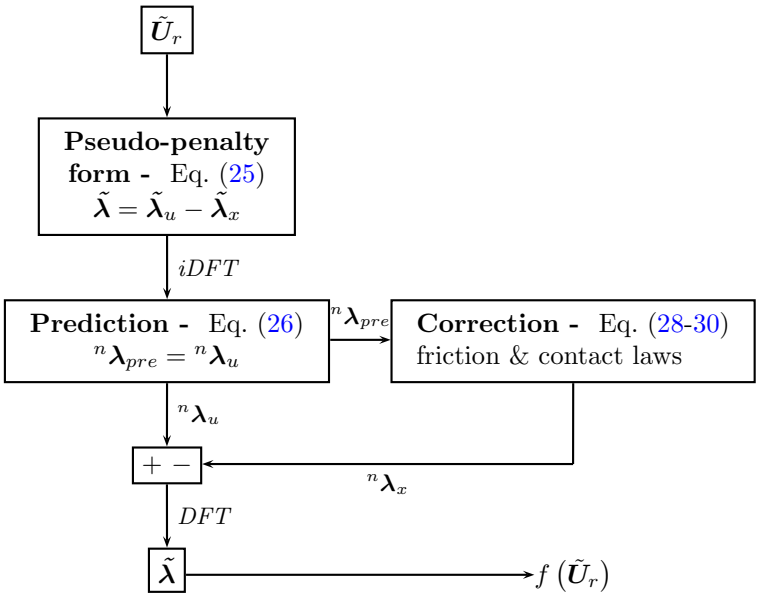

Figure 2. Computation of the Lagrangian vector with wear

1. Separation: $\lambda_{pre}^{n,N} \geq 0$
   The contact is lost and the forces should be zero.

$$\boldsymbol{\lambda_x^n} = \boldsymbol{\lambda_u^n}. \tag{28}$$

2. Stick: $\lambda_{pre}^{n,N} < 0$ and $\left\|\boldsymbol{\lambda_{pre}^{n,T}}\right\| < \mu \left|\lambda_{pre}^{n,N}\right|$
   In this case, the prediction verifies the contact conditions:

$$\lambda_x^{n,N} = 0, \quad \boldsymbol{\lambda_x^{n,T}} = \boldsymbol{\lambda_x^{n-1,T}}. \tag{29}$$

3. Slip: $\lambda_{pre}^{n,N} < 0$ and $\left\|\boldsymbol{\lambda_{pre}^{n,T}}\right\| \geq \mu \left|\lambda_{pre}^{n,N}\right|$
   Again, there is no normal relative displacement. The correction is made assuming that the tangential contact force has the same direction as the tangential predicted force. The definition of relative velocity and the respect of the Coulomb's law give:

$$\lambda_x^{n,N} = 0, \quad \boldsymbol{\lambda_x^{n,T}} = \boldsymbol{\lambda_x^{n-1,T}} + \boldsymbol{\lambda_{pre}^{n,T}} \left(1 - \mu \frac{\left|\lambda_{pre}^{n,N}\right|}{\|\boldsymbol{\lambda_{pre}^{n,T}}\|}\right). \tag{30}$$

The final step consists of transforming back the time domain updated Lagrangian in the frequency domain using the DFT algorithm.

3.3. Wear depth calculation

At the end of the iDFT/DFT internal loop, it becomes possible to calculate the nodal wear for a single fretting cycle, denoted δW_1^M, by wear rate integration:

$$\delta W_1^M(\eta) = \frac{K_w}{\alpha^M} \int_{\eta}^{\eta+T} \left|P_N^M(\tau,\eta)\right| \left\|\dot{\boldsymbol{U}}_T^M(\tau,\eta)\right\| d\tau. \tag{31}$$

The interface gap - i.e. the geometry - can then be updated. In practice, to accelerate the calculation by decreasing the number of slow time steps, it is necessary to jump a certain number of cycles between two steps.

The considered duration of the study, T, is split into k intermediate slow time steps. A too important step would provoke such an unbalance in the contact zone that a high number of loops in the prediction/correction process would be required to compensate for it. k is chosen heuristically as the probably best compromise between the total number of slow-time steps and the number of required prediction-correction loops.

Concerning the evolution of wear depths, the integration follows an explicit scheme:

$$\boldsymbol{W}^M(\eta^{k+1}) = \boldsymbol{W}^M(\eta^k) + \frac{\eta^{k+1} - \eta^k}{T}\,\delta W_1^M(\eta^k). \tag{32}$$

At the level of the contact, equilibrium conditions are then modified: this imposes a return back to the beginning of the prediction/correction process to re-equilibrate them. Then, a new loop - the wear updating loop or intermediate loop - appears in the algorithm. This is specific to the DLFT-with-wear method.

The strategy of the DLFT-with-wear method is summarized in Fig. 3. One can notice the three loops mentionned above, whereas the "classical" DLFT has only two loops.

4. Numerical example

4.1. Description of the model

The algorithm developed for the coupled calculation of both the wear kinetics and the vibratory response has been applied to a beam. This beam is parallelepipedic with length $L = 100\,mm$, width $l = 10\,mm$ and thickness $h = 10\,mm$ (Fig. 4). It is made of steel. The material's properties are $E = 210\,GPa$, $\nu = 0.3$, $\rho = 7,800\,kg/m^3$ and the damping factor is $\eta = 0.001$. The structure is connected to the ground by a spring of stiffness $\beta = 0.01\,MN/m$ in the $\mathbf{x}$ direction. It lies on a rigid support with unilateral contact conditions. The initial gap is zero. The friction coefficient is $\mu = 0.3$ and Archard's law wear coefficient is $k_w = 1.10^{-11}\,Pa^{-1}$. It is subjected to a normal load P fixed at $0.01\,MPa$ and to a sinusoidal load Q. Q's amplitude is $0.01\,MPa$.

Two cases are treated according to the frequency of excitation. In the first case, the loading is supposed to be quasi-static, ie the frequency is low compared to the first resonance frequency of the system and inertial phenomena are neglected. A resembling example was studied by Strömberg [19], it will then be possible to verify qualitatively the results. This case is considered for the sake of comparison with the second case, for which the frequency is more important, entailing that dynamical aspects must be taken into account.

For both cases, the beam is discretized into linear 2D finite elements under the assumption of plane strains. Each element has four nodes with two degrees of freedom per node. The harmonic balance uses 7 harmonics. Each considered cycle is discretized into 128 time-steps in the DFT correction procedures.

4.2. Case of a quasi-static loading

The evolution of wear depth is drawn in Figs. 5 and 6. The worn profile is drawn for the initial cycle, three intermediate numbers of cycles and for a number of cycles for which a steady state has been apparently reached. Three kinds of behaviour appear: no wear occurs in the zone closest to the fastening spring; maximal wear depths are reached in the zone where the oscillating load is applied; an intermediate zone separates the no-wear zone and the maximal-wear zone, it progressively goes from the stick state to the slip state. These results are qualitatively in good agreement with Strömberg's ones [19].

With the view of better understanding the wear process, the evolution of the wear depth as the cycles go by is drawn for some points which belong on the one hand to the initial zone of slip (Fig. 7) and on the other hand to the intermediate zone (Fig. 8). Fig. 7 shows that in the initial slip zone wear is intense at the beginning of the process, but when the local normal pressures relax (Fig. 10), wear rates tend to zero. Fig. 8 reveals more complex wear kinetics. Due to the increase of wear in the sliding zone, the amplitude of the local normal pressure progressively increases in the transition zone between stick and slip. Equilibrium conditions then impose a release of the normal pressure in the sticked zone closest to the peak of normal pressure. This zone is then likely to become a sliding zone, where wear occurs. Such phenomena of normal

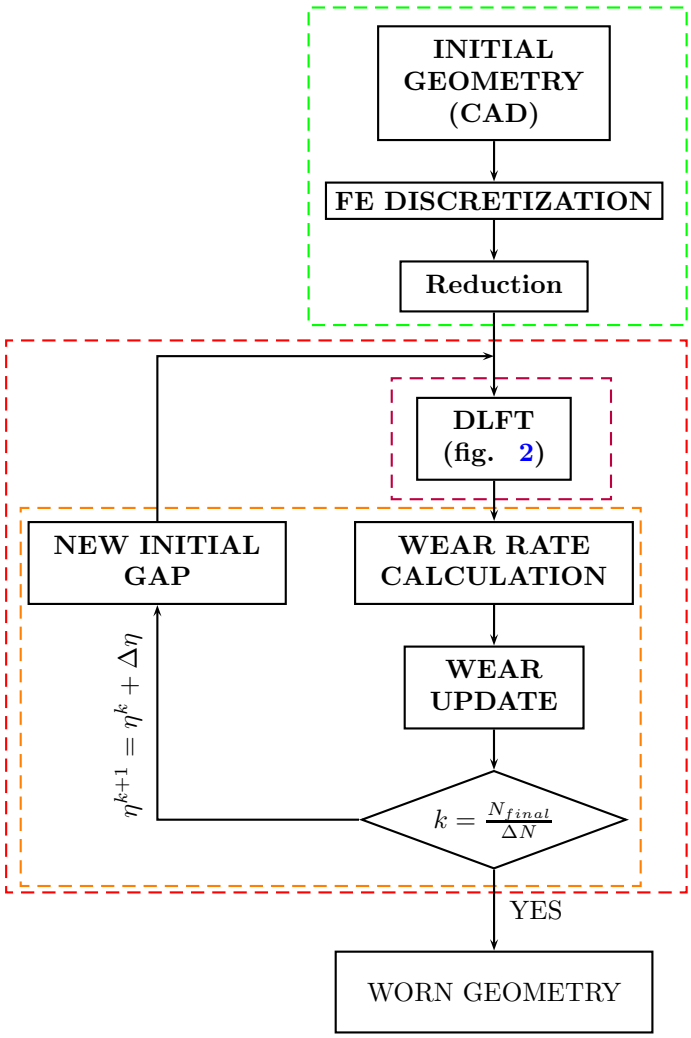

Figure 3. Global flow chart of the DLFT-with-wear method: – model creation, – DLFT-with-wear procedure, – DLFT algorithm and – wear calculation.

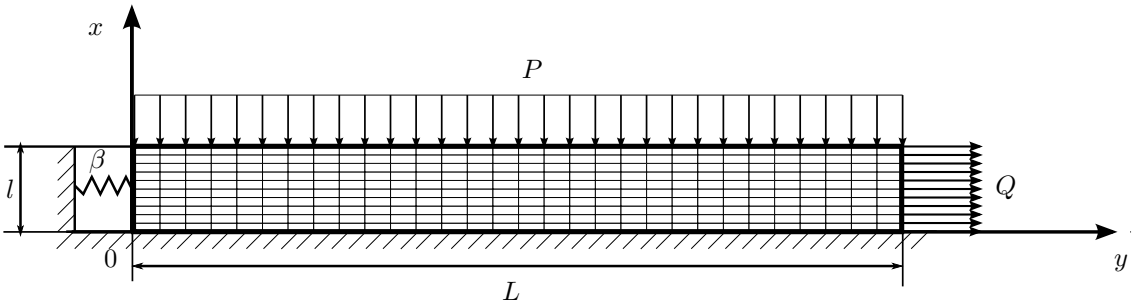

Figure 4. Geometry, boundary conditions and mesh of the studied beam

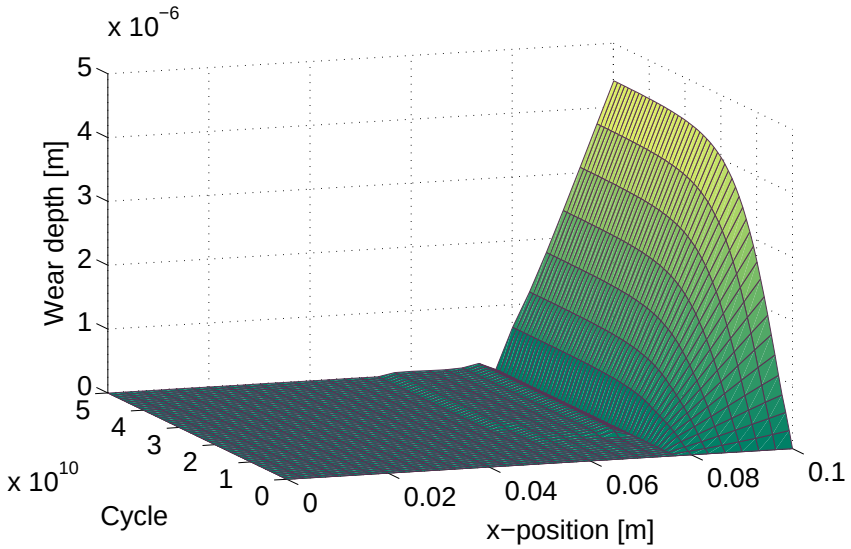

Figure 5. Wear depth evolution (quasi-static case)

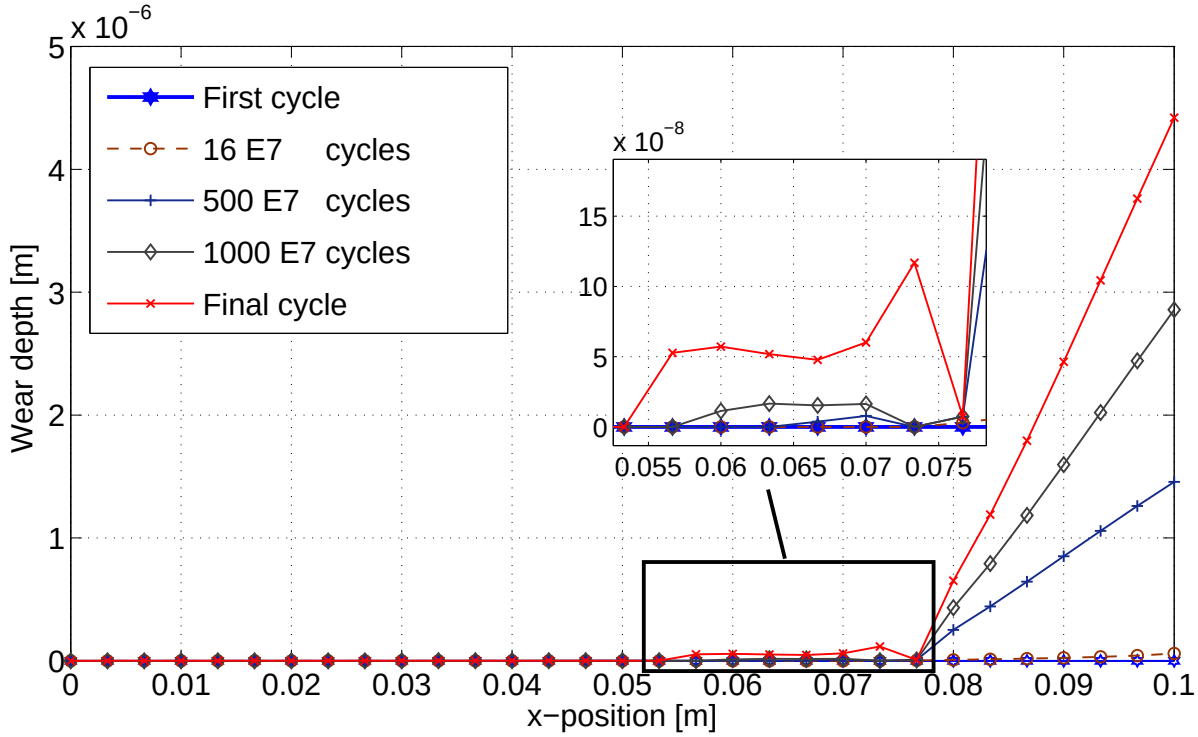

Figure 6. Excerpt of Fig. 5: wear profile for 5 particular numbers of cycles

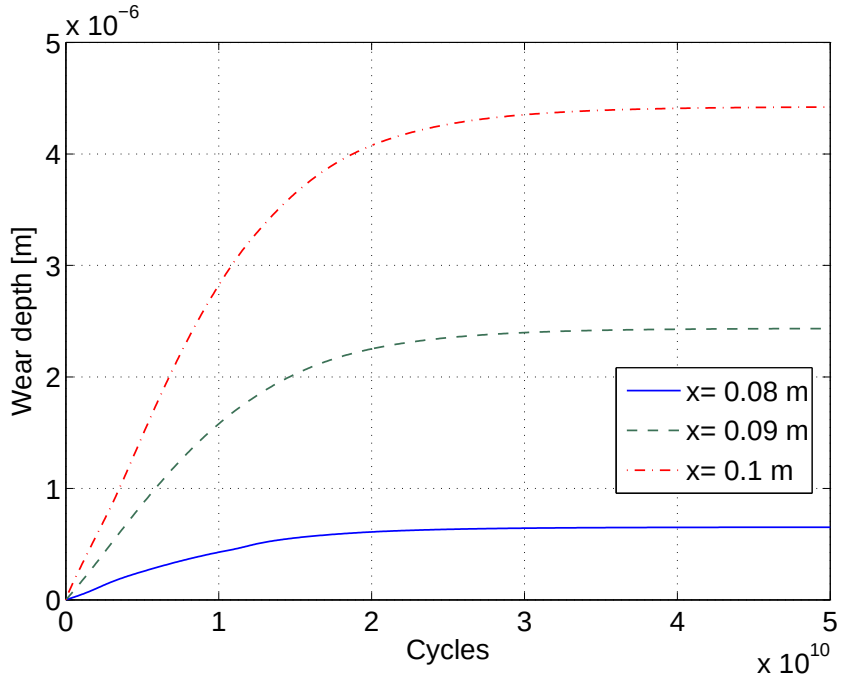

Figure 7. Excerpt of Fig. 5: evolution of wear in the slip zone

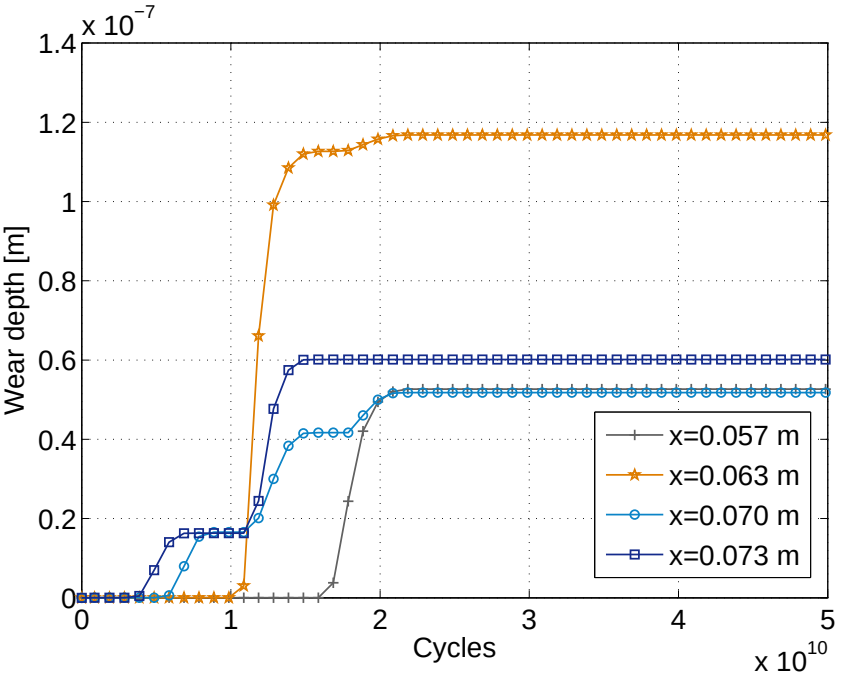

Figure 8. Excerpt of Fig. 5: evolution of wear in the intermediate zone

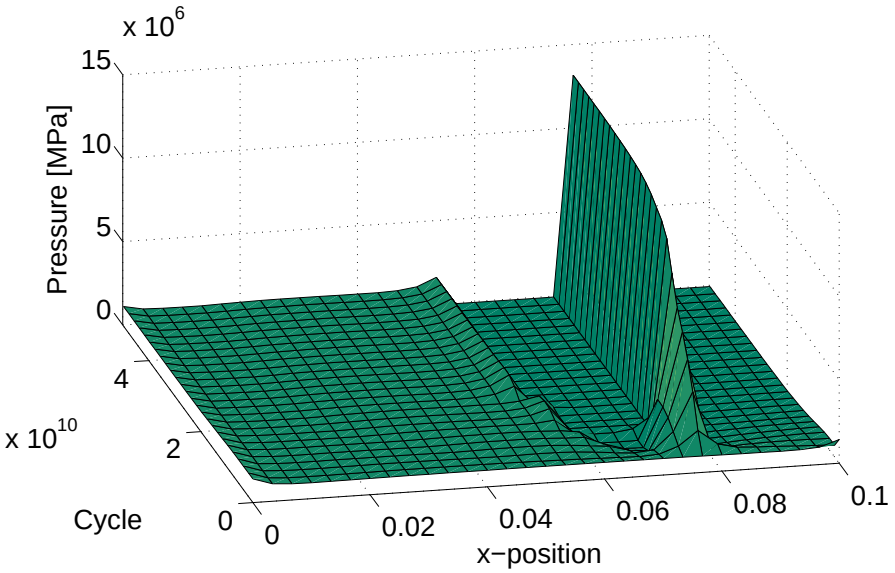

Figure 9. Evolution of amplitude of the normal contact pressure distribution

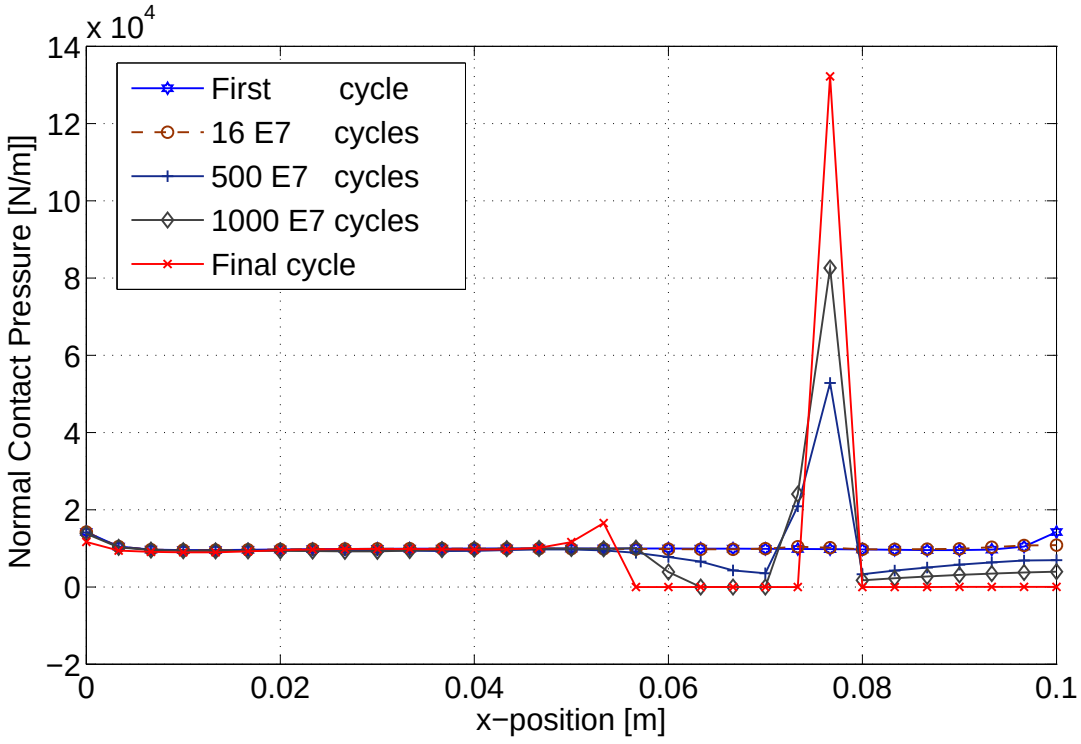

Figure 10. Amplitude of the normal contact pressure distribution for 5 particular numbers of cycles (quasi-static case)

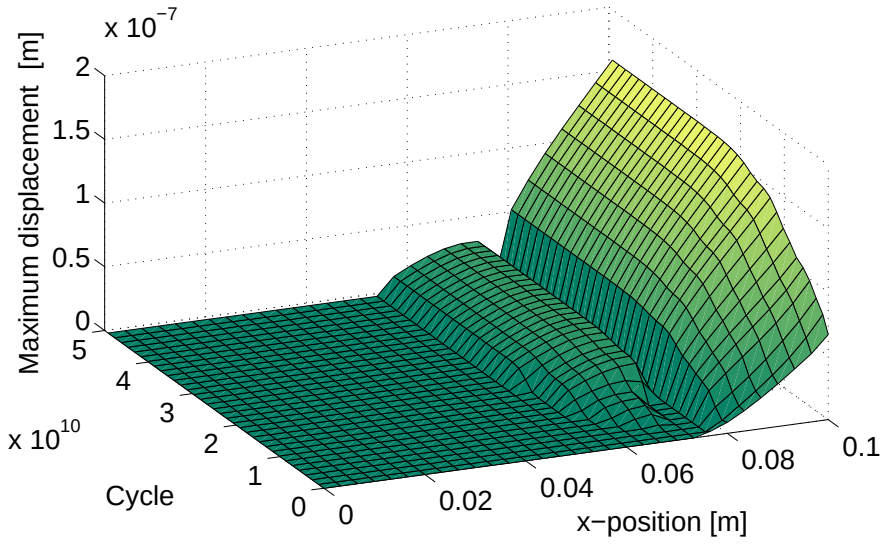

Figure 11. Evolution of the amplitude of the horizontal displacement in the contact zone (quasi-static case)

pressure redistribution make that, during the cycles, wear sometimes stops and sometimes restarts after a few cycles.

Moreover, a little zone seems to never wear out. It is characterized by a null sliding (Fig. 11 and Fig. 12) and a high level of normal pressure (Fig. 10). This null-wear node plays the role of a "pillar" which would be responsible for the steady-state regime, with a null wear rate, that the system seems to reach.

This example will be used in the next section as a reference while examining how inertial effects affect the wear process.

4.3. Case of dynamical loadings

To start with, the vibratory behaviour of the beam without wear is explored, for different contact types, via the calculation of the frequency response function (FRF) giving the amplitude of the horizontal displacement at the node P_e located at the extremity of the beam and at the level of the contact ($x = L$, $y = 0$). The frequency range goes from $1\,Hz$ to $100\,kHz$. The FRF is obtained through the DLFT algorithm (Fig. 13). Four modes are observed for a free interface without friction against two modes for a blocked interface. The case with a frictional interface reveals an intermediate behaviour, strongly damped, with a big non-linear resonance at $30\,kHz$ and two smaller at $70\,kHz$ and $81\,kHz$ (Fig. 14).

Fig. 15 shows the final worn profiles obtained for some particular frequencies spotted in Fig. 14.

Compared to the quasi-static case, the introduction of inertial effects gives infinitely various behaviours, since they depend on the frequency. This is illustrated here for $f = 10\,kHz$ and $f = 79\,kHz$ (Fig. 16). The node considered before, P_e, stops two times per period at $f = 10\,kHz$ and four times per period at $f = 79\,kHz$. Such situations are well known for a single degree of freedom Coulomb friction oscillator [29].

From now on, wear is taken into account. Since the initial dynamical behaviour depends on the frequency, wear also depends on it: the study focuses on the excitation at $f = 79\,kHz$. The computation is performed using a simple explicit Euler scheme on the slow scale and the DLFT method inside the vibratory periods.

The displacements along the contacting zone of the beam evolve according to the cycles as shown on Fig. 17 and Fig. 18: progressively, almost all the points come to move. But in two zones, around $x = 0.005\,m$ and between $x = 0.025\,m$ and $x = 0.040\,m$, nodes of vibration seem to appear, accompanied by an increase of the amplitude of the normal contact pressure (Fig. 19) and by a null wear depth (Fig. 20 and Fig. **??**).

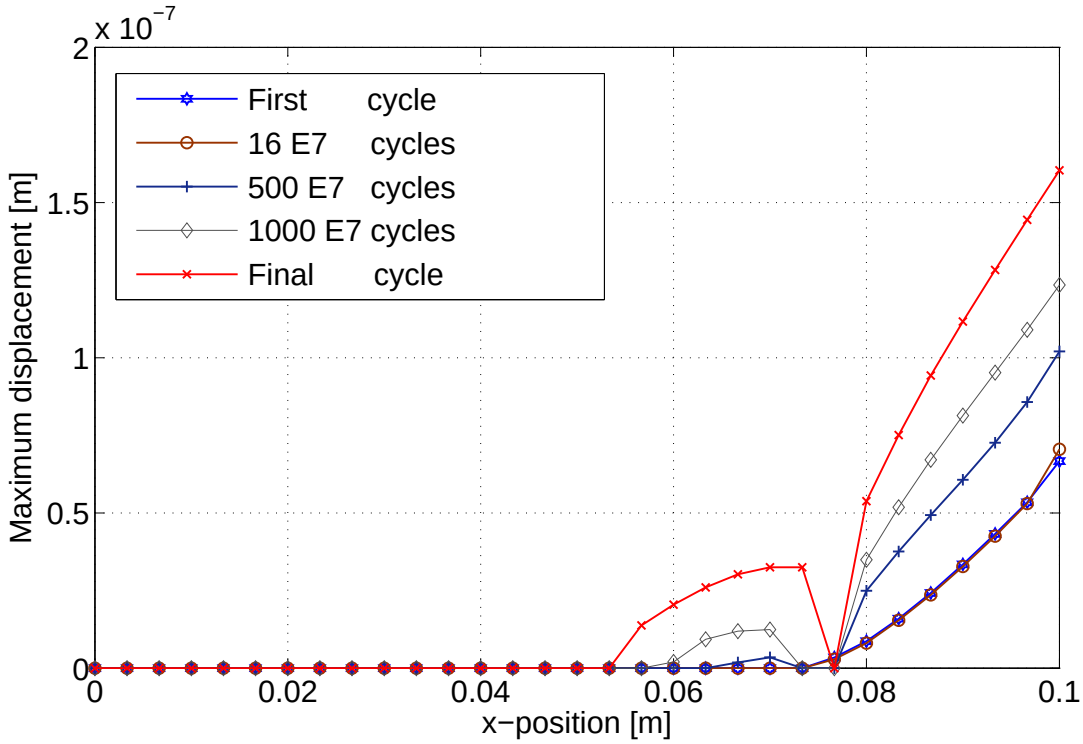

Figure 12. Excerpt of Fig. 5: displacement amplitude for 5 particular numbers of cycles

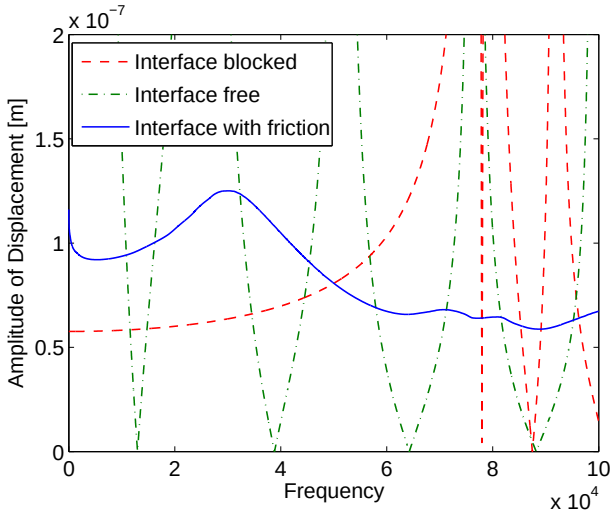

Figure 13. FRF of the horizontal displacement of P_e with different contact types

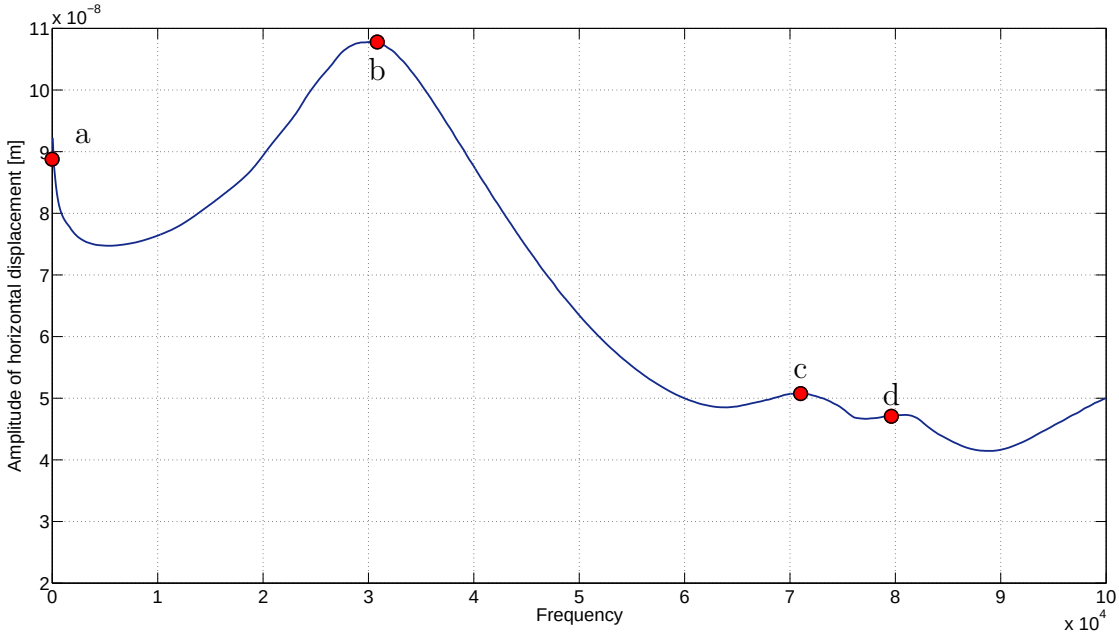

Figure 14. Zoom on Fig. 13 for a frictional interface

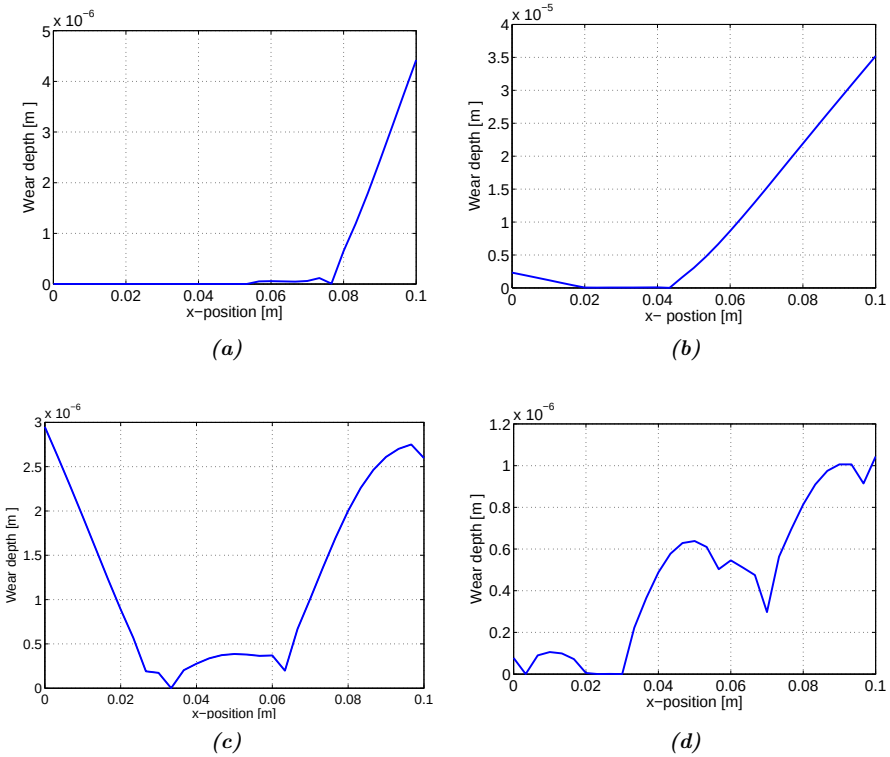

Figure 15. Final worn profile for different frequencies: (a) quasi-static, (b) $f = 30kHz$, (c) $f = 70kHz$ and (d) $f = 79kHz$

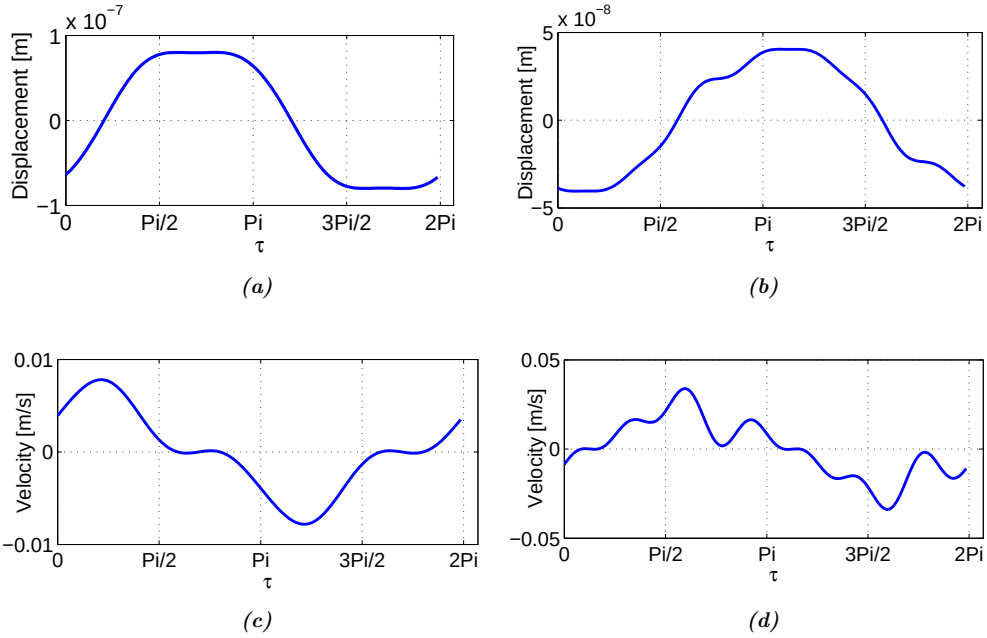

Figure 16. Displacement and velocity of P_e versus $\tau = \omega t$: $f_1 = 10kHz$ (a) and $f_4 = 10kHz$ (a).

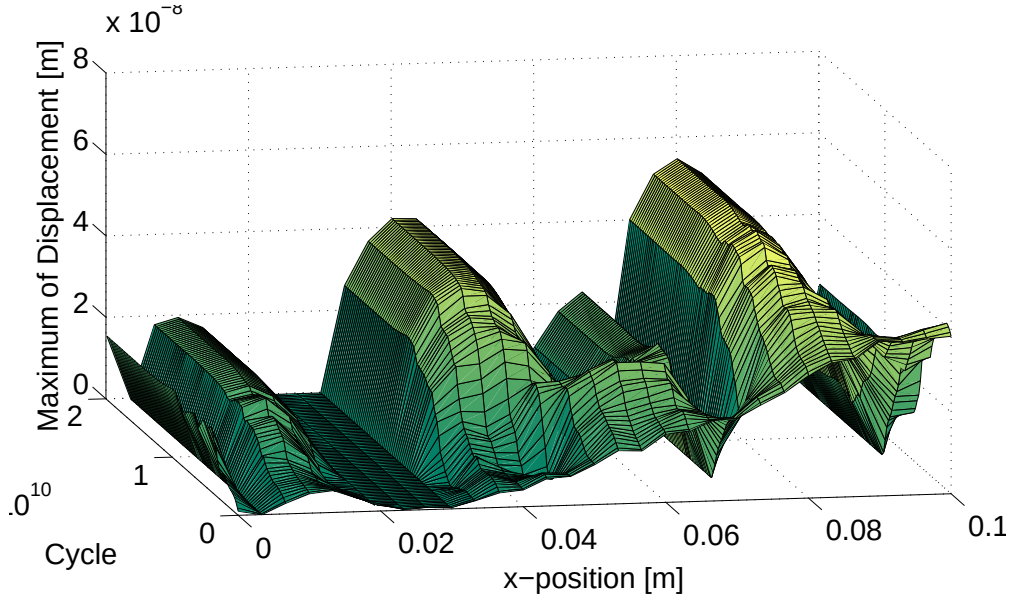

Figure 17. Evolution of the amplitude of the horizontal displacement in the contact zone ($79kHz$)

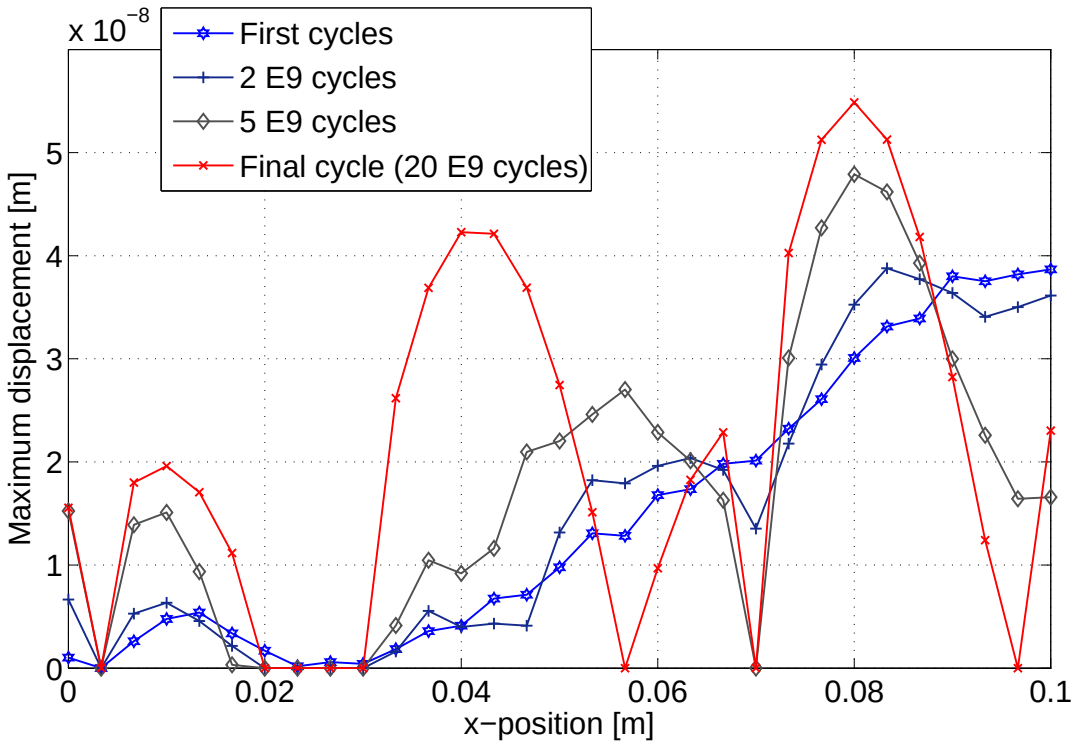

Figure 18. Excerpt of Fig. 17: displacement amplitude for 4 particular numbers of cycles

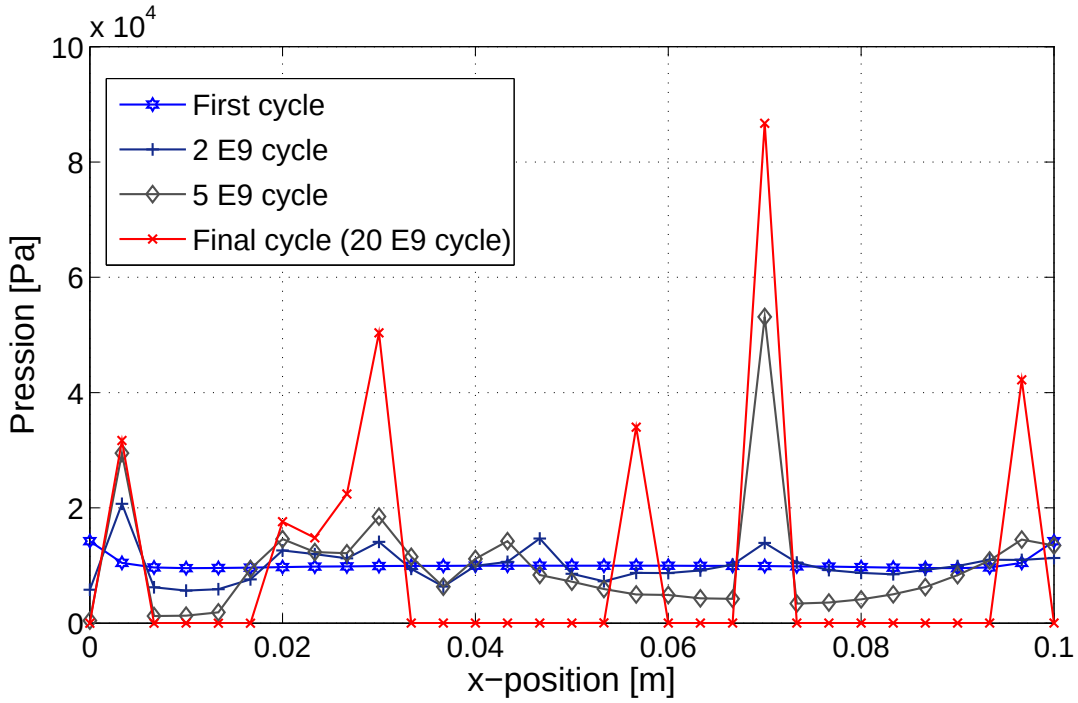

Figure 19. Amplitude of the normal contact pressure distribution for 4 particular numbers of cycles ($79kHz$)

Example	New. it. / cycle	CPU time / cycle	total New. it.	total cycle nb	total CPU time
quasi-static	2.96	0.57 s	4474	1510	861 s
79 kHz	2.32	1.02 s	13977	6007	6127 s

Table 1. Statistics about the performance of the DLFT-with-wear method

The explanation of this phenomenon is analogous with the one suggested in the quasi-static analysis, but the equilibrium conditions that determine the modifications of the pressure distribution are here dynamical conditions, hence the "pillar" evoked in quasi-static conditions is replaced here by nodal zones of vibration. The worn geometry profile is consequently very different from the one observed in quasi-static conditions. Finally, the evolution of the total worn volume seems to reveal that a steady-state is reached in the dynamical case too (Fig. 21).

4.4. Comments on the numerical performance of the DLFT-with-wear method

The algorithm is implemented in Matlab R2009 environment on a Linux PC with an Intel Core i7 920 (2.66 GHz) CPU. Some statistics about the time costs of the algorithm are provided in Tab. 1.

It is important here to remind that many wear cycles are skipped, because the evolution of the worn profile during a single cycle is very limited. Therefore, the wear integration procedure, on the slow time scale, is based, through an Euler explicit scheme, on increments whose maximum value is set at $1E8$ cycles for the quasi-static case and at $1E7$ cycles for the $79kHz$ case (to ensure the convergence). The total number of cycles actually dealt with the non-linear algorithm is then much lesser than the total number of cycles physically addressed. The cycles mentionned in the table are only the ones actually computed in the non-linear procedure.

The second column gives the average number of iterations required by the Newton solver in the DLFT-with-wear algorithm for the whole range of cycles the calculation deals with. A low number of iterations

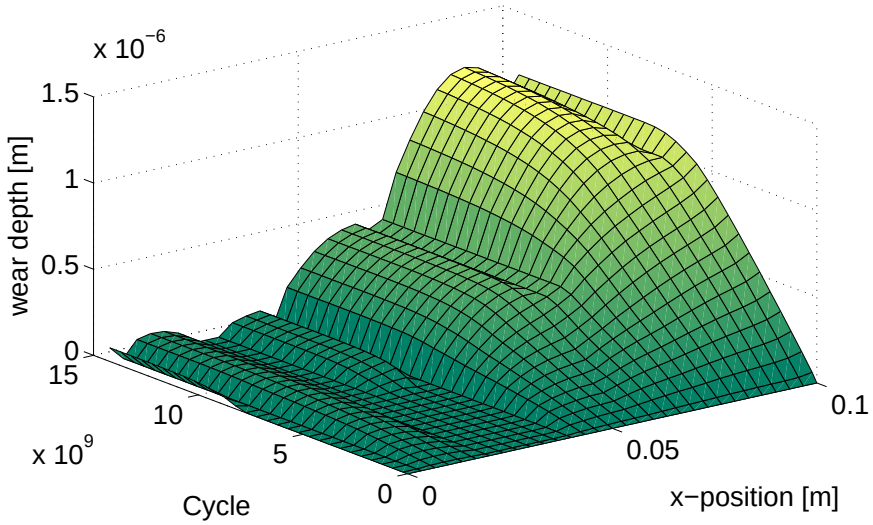

Figure 20. Wear depth evolution ($79kHz$)

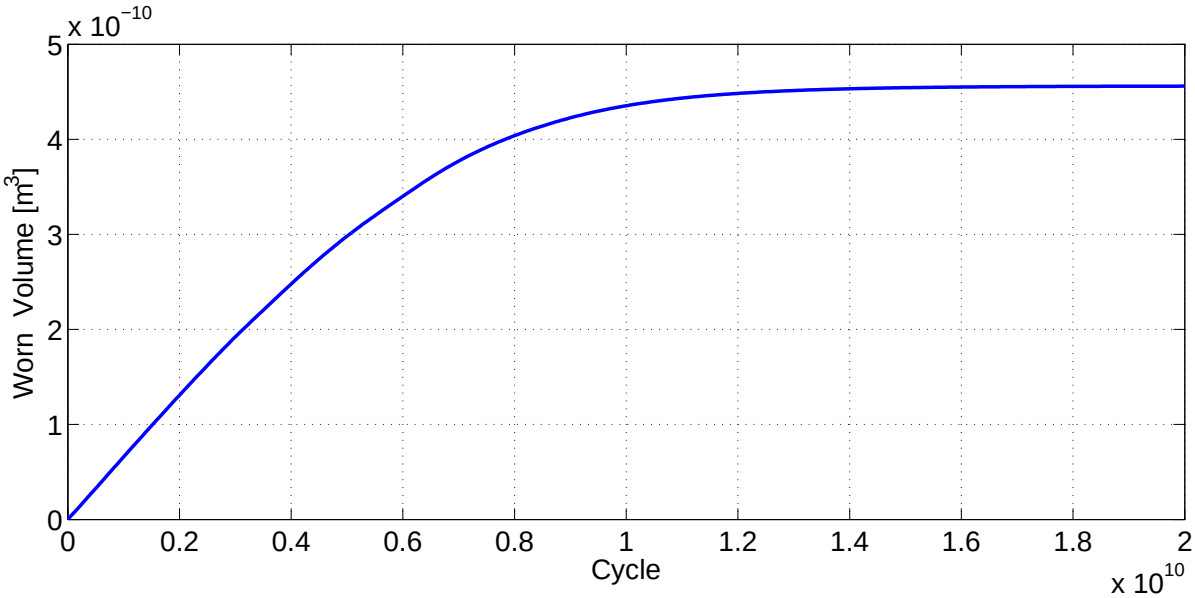

Figure 21. Total worn volume evolution ($79kHz$)

is generally enough but a maximum of 15 iterations has been observed. The third column shows that, on average, it is longer, in terms of CPU time, to reach convergence for a dynamical behaviours than for a quasi-static behaviour. The other columns confirm this tendency. The evaluation of fretting-wear under vibrations is consequently a more time consuming procedure.

5. Conclusions and prospects

In this paper, a method has been proposed to calculate simultaneously the wear and the vibrations of structures in situation of fretting-wear. It is based on the assumption that dynamical and tribological phenomena can be separated on two time scales. The vibrations are analysed in the frequency domain through harmonic balance and AFT procedures. The evolution of wear is integrated on a slow time scale through an explicit scheme coupled with a skip cycles approach. The algorithm uses hybrid Powell's solver to deal with the issuing non-linear system.

The tests performed on a two dimensional case show a good concordance between the DLFT-with-wear method and a method stemming from the literature in the quasi-static case. Nevertheless, the comparison of the quasi-static forced response with its dynamical counterparts, including inertia at different frequencies, reveal on the one hand the importance of the coupling between dynamics and wear and on the other hand the complexity of wear kinetics. Indeed, despite wear depths are very small (a few microns), they modify a lot the vibratory behaviour of the structure. That is why it is strongly recommended that designers take this parameter into account when they dimension structures subject to freeting-wear and vibratory loads. They can use the method presented here, but, of course, calibration tests must be performed to guarantee that the life expectancy calculations are faithful to reality.

To conclude, a steady state with null wear rate has been picked out on the example. In the future, this observation may give rise to another method, potentially based on an optimization process, which would enable one to know rapidly an asymptotic worn geometry, if it exists.

Acknowledgments

Thanks go to Snecma for its technical and financial support. This work takes place in the framework of the MAIA mechanical research and technology program sponsored by CNRS, ONERA and SAFRAN Group.

References

[1] D. Charleux, C. Gibert, F. Thouverez, J. Dupeux, Numerical and Experimental Study of Friction Damping in Blade Attachments of Rotating Bladed Disks, International Journal of Rotating Machinery 2006 (2006) 1–13.
[2] E. P. Petrov, D. J. Ewins, Analytical Formulation of Friction Interface Elements for Analysis of Nonlinear Multi-Harmonic Vibrations of Bladed Disks, Journal of Turbomachinery 125 (2003) 364–371.
[3] S. Nacivet, C. Pierre, F. Thouverez, L. Jézéquel, A dynamic Lagrangian frequency–time method for the vibration of dry-friction-damped systems, Journal of Sound and Vibration 265 (1) (2003) 201–219.
[4] G. Levy, Modeling of Coulomb Damping and Wear of Vibrating Systems, Wear 64 (1) (1980) 57–82.
[5] W. Sextro, Dynamical Contact Problems With Friction: Models, Methods, Experiments, and Applications, Springer, 2002.
[6] H. C. Meng, K. C. Ludema, Wear models and predictive equations: their form and content, Wear 181 (2) (1995) 443–457.
[7] J. F. Archard, Contact and rubbing of flat surfaces, Journal of Applied Physics 24 (8) (1953) 981–988.
[8] I. R. McColl, J. Ding, S. B. Leen, Finite element simulation and experimental validation of fretting wear, Wear 256 (11) (2004) 1114–1127.
[9] C. Mary, S. Fouvry, Numerical prediction of fretting contact durability using energy wear approach: Optimisation of finite-element model, Wear 263 (2007) 444–450.
[10] P. Põdra, S. Andersson, Wear simulation with the Winkler surface model, Wear 207 (1997) 79–85.
[11] L. Gallego, D. Nélias, C. Jacq, A Comprehensive Method to Predict Wear and to Define the Optimum Geometry of Fretting Surfaces, Journal of Tribology 128 (2006) 476–485.
[12] G. K. Sfantos, M. H. Aliabadi, Wear simulation using an incremental sliding Boundary Element Method, Wear 260 (2006) 1119–1128.
[13] G. K. Sfantos, M. H. Aliabadi, Application of BEM and optimization technique to wear problems, International Journal of Solids and Structures 43 (2006) 3626–3642.

[14] J. Guillen, C. Pierre, An efficient, hybrid, frequency-time domain method for the dynamics of large-scale dry friction damped structural systems, in: IUTAM Symposium on Unilateral Multibody Contacts, Kluwer Academic Pub, 1999.
[15] G. Csaba, Forced response analysis in time and frequency domains of a tuned bladed disk with friction dampers, Journal of Sound and Vibration 214 (3) (1998) 395–412.
[16] S. Fouvry, T. Liskiewicz, P. Kapsa, S. Hannel, E. Sauger, An energy description of wear mechanisms and its applications to oscillating sliding contacts, Wear 255 (1-6) (2003) 287–298.
[17] L. Salles, L. Blanc, F. Thouverez, A. M. Gouskov, Dynamic Analysis of Fretting-Wear in Friction Contact Interfaces , in: Proceedings of ASME Turbo Expo, 2008.
[18] L. Salles, L. Blanc, F. Thouverez, A. M. Gouskov, P. Jean, Dynamic Analysis of a Bladed Disk with Friction and Fretting-Wear in Blade Attachements, in: Proceedings of ASME Turbo Expo, 2009.
[19] N. Stromberg, An augmented Lagrangian method for fretting problems, European Journal of Mechanics. A. Solids 16 (4) (1997) 573–593.
[20] A. H. Nayfeh, D. T. Mook, Nonlinear Oscillations, Wiley, 1979.
[21] L. Meirovitch, Methods of Analytical Dynamics, Dover Publications, 2004.
[22] J. P. Cusumano, A. Chatterjee, Steps towards a qualitative dynamics of damage evolution, International Journal of Solids and Structures 37 (44) (2000) 6397–6417.
[23] H. Demiray, E. Brommundt, A simple mechanism for the polygonalization of railway wheels by wear, Mechanics Research Communications 24 (4) (1997) 435–442.
[24] T. M. Cameron, J. H. Griffin, An alternating frequency/time domain method for calculating the steady-state response of nonlinear dynamic systems, ASME, Transactions, Journal of Applied Mechanics 56 (1989) 149–154.
[25] E. P. Petrov, D. J. Ewins, Models of friction damping with variable normal load for time-domain analysis of vibrations, in: Proceedings of the International Conference on Noise and Vibration Engineering (ISMA), Leuven, 2002.
[26] O. Poudou, C. Pierre, Hybrid frequency-time domain methods for the analysis of complex structural systems with dry friction damping, in: Collection of Technical Papers - AIAA/ASME/ASCE/AHS/ASC Structures, Structural Dynamics and Materials Conference, 2003, pp. 111–124.
[27] E. Ciğeroğlu, H. N. Özgüven, Nonlinear vibration analysis of bladed disks with dry friction dampers, Journal of Sound and Vibration 295 (2006) 1028–1043.
[28] D. Laxalde, F. Thouverez, J. J. Sinou, J. P. Lombard, Qualitative analysis of forced response of blisks with friction ring dampers, European Journal of Mechanics/A Solids 26 (4) (2007) 676–687.
[29] H. K. Hong, C. S. Liu, Coulomb friction oscillator: modelling and responses to harmonic loads and base excitations, Journal of Sound and Vibration 229 (5) (2000) 1171–1192.